Elasticity generates indissoluble biomolecular condensates

Lingyu Meng[1] and Jie Lin[1, 2]
[1] *Peking-Tsinghua Center for Life Sciences, Peking University, Beijing, China*
[2] *Center for Quantitative Biology, Peking University, Beijing, China*

(Dated: February 10, 2022)

While biomolecular condensates are often liquid-like, many experiments found that condensates also exhibit solid-like behaviors, which may make them irreversible and indissoluble. Despite the critical biological significance of indissoluble condensates to cellular fitness and diseases, the physical mechanisms underlying the stabilities of solid-like condensates are still unclear. In this work, we study the effects of elasticity on the dissolution of biomolecular condensates. We demonstrate that the bulk stress inside condensates may prevent the condensates from dissolution and obtain the new equilibrium conditions of elastic condensate: the osmotic pressure minus the bulk stress is uniform inside and outside condensates. To verify our theories, we simulate the two-fluid model in which the slow component corresponding to the polymer network generates elastic stress. Our theoretical predictions are nicely confirmed and independent of microscopic details. Moreover, we obtain a phase diagram on the stability of elastic condensates and identify a minimum bulk modulus for the condensates to be indissoluble, both numerically and theoretically. Our results may have implications in developing drugs targeting irreversible condensates.

Biomolecular condensates are widely observed in various organisms, usually composed of proteins and RNAs [1–9]. They often have crucial biological functions [10, 11], such as adaptive responses to stresses, accelerating biochemical reactions, and sequestering molecules from reactions. Therefore, the accurate regulation of biomolecular condensates' formation and dissolution is critical. Meanwhile, experiments have also found that biomolecular condensates are viscoelastic rather than completely viscous [12]: they are solid-like on a short time scale and liquid-like on a long time scale. More interestingly, they exhibit aging behaviors, and the viscoelastic relaxation time, which separates solid and liquid behaviors, increases over time [13]. Indeed, aged condensates may become indissoluble or infusible in conditions where newly formed condensates can easily dissolve or fuse [3, 4, 7, 9, 14–18]. Moreover, indissoluble condensates may affect cellular fitness, e.g., failure to dissolve condensates during mitosis leads to aberrant condensates that cause the cell-cycle arrest and ultimately cell death [19]. In general, indissoluble condensates are believed to lead to aging at the cellular or organismic level and are related to multiple diseases [15, 20–22].

Theoretical studies on the formation and dissolution of biomolecular condensates have so far been limited to fluid models, in which the elastic nature of condensates are usually neglected [23]. Meanwhile, numerous experiments have demonstrated the importance of solid-like nature on the dissolution of condensates [13, 22], and our theoretical understanding of this problem is still in its infancy. In this work, we seek to fill this gap and investigate the effects of elasticity on the dissolution and stability of biomolecular condensates, combining both analytical theories and computer simulations. In the following, we first introduce our theoretical frameworks focusing on elastic condensates that are subject to an abrupt parameter change. Without elasticity, they are supposed to dissolve. We then derive the equilibrium conditions for elastic condensates and find that the bulk stress plays an essential role in preventing the dissolution. A finite bulk modulus may render the condensate irreversible and indissoluble. To test our theoretical predictions, we simulate the two-fluid model [24, 25] beyond the traditional fluid model of phase separation dynamics (Model H) [23, 26], by including elastic stress generated by the polymer network. Our theories are nicely confirmed and valid independent of the microscopic details, such as the free energy form. Furthermore, we provide a phase diagram of condensate stability and demonstrate a minimum bulk modulus for the condensate to be indissoluble. Finally, we discuss the biological implications of our work and propose future directions to explore.

Equilibrium conditions of elastic condensates

Biomolecular condensates usually have well-defined viscoelastic relaxation times, below which the condensates behave as elastic materials [12, 13]. In this work, we simplify the problem by considering an aged condensate with its viscoelastic relaxation time much longer than the time scales of biological interests, e.g., the duration of cell-cycle phases. Therefore, its viscoelastic relaxation time can be taken as infinite, which is the main focus of this work (Figure 1). We introduce an abrupt change to the attractive interaction between the monomers of biomolecules, either due to environmental change, e.g., an increase in temperature, or active cellular regulation, e.g., post-translational phosphorylation. In the absence of elasticity, the condensate will dissolve. However, as we show in the following, the elastic force may prevent the dissolution.

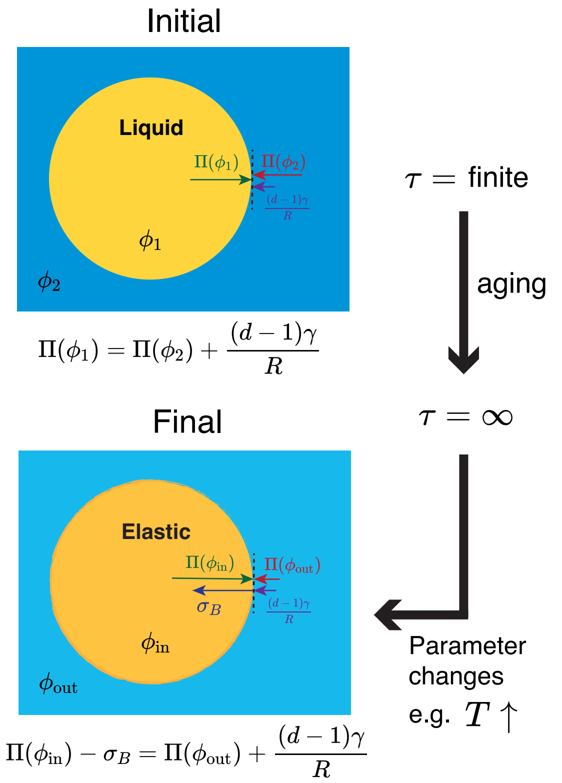

FIG. 1. Equilibrium conditions of elastic condensates. Liquid-like condensates are initially formed from liquid-liquid phase separation, which then become aged and solid-like. An abrupt change in the effective attractive interaction between biomolecular monomers is introduced, e.g., through an increase in temperature or post-translational modification. The bulk stress σ_B in the condensate is involved in the new equilibrium condition to prevent dissolution.

In liquid-liquid phase separation, a stable condensate requires the Gibbs-Thomson relation of osmotic pressure: $\Pi_{\rm in} = \Pi_{\rm out} + (d-1)\gamma/R$. Here, $\Pi_{\rm in\ (out)}$ is the osmotic pressure inside (outside) the condensate, γ is the surface tension constant, d is the spatial dimension and R is the condensate radius. In this work, we propose the following equilibrium condition for elastic condensates (see detailed derivations in Methods),

$$\Pi_{\rm in} - \sigma_B = \Pi_{\rm out} + \frac{(d-1)\gamma}{R}, \qquad (1)$$

Here σ_B is the bulk stress inside the condensate (Figure 1). As we show later, the inclusion of bulk stress compensates the imbalance of osmotic pressures. To find the expression of σ_B, we use the constitutive equation of the bulk stress and the continuity equation of density (ϕ)

$$\frac{\partial \sigma_B}{\partial t} = G_B \nabla \cdot \mathbf{v_p}, \qquad (2)$$

$$\frac{\partial \phi}{\partial t} = -\phi \nabla \cdot \mathbf{v_p}. \qquad (3)$$

Here $\mathbf{v_p}$ is the velocity field of the polymer, e.g., proteins, which is responsible for the bulk stress. G_B is the bulk modulus. In writing the above two equations, we assume that ϕ and σ_B are uniform inside the condensate, which we confirm numerically later. Combining Eqs. (2, 3), we obtain

$$\sigma_B = G_B \ln\left(\frac{\phi_1}{\phi_{\rm in}}\right) \qquad (4)$$

where ϕ_1 and $\phi_{\rm in}$ are respectively the densities of the condensate before and after the condition changes.

We note that to uniquely determine the density inside and outside the condensate, $\phi_{\rm in}$ and $\phi_{\rm out}$, we still need one more equation. For liquid condensates, it is a uniform chemical potential. However, in our case, the condensate is solid; therefore, the exchange of molecules is suppressed [3, 8, 22]. Instead, we propose that condensate size does not change upon the weakening of attractive interaction between biomolecules' monomers, namely, $R = R_0$, where R and R_0 are respectively the radii of elastic condensate before and after the condition changes. We confirm this assumption numerically later. Given R and $\phi_{\rm in}$, $\phi_{\rm out}$ can be calculated using the conservation of total molecular number: $V\phi_0 = \sum_i V_i \phi_{{\rm in},i} + (V - \sum_i V_i)\phi_{\rm out}$. Here V is the total volume, V_i is the volume of condensate i, and the summation is over all condensates. ϕ_0 is the average density over the total volume. Finally, we remark that in our case, the bulk stress inside the condensate stabilizes the condensate, in contrast to the bulk stress outside a condensate, e.g., due to the surrounding polymer network that suppresses the formation of condensates [27–29].

Numerical simulations

In the following, we numerically simulate the two-fluid model in two dimensions [24, 25] to test our theories with two components: the slow component corresponding to the polymer and the fast component corresponding to the solvent. It is the polymer component that generates the elastic stress. The average velocity field $\mathbf{v} = \phi\mathbf{v_p} + (1-\phi)\mathbf{v_s}$ where $\mathbf{v_p}$ are $\mathbf{v_s}$ are respectively the polymer and solvent velocity field. The dynamics of polymer density and velocity field follows (see details in Methods)

$$\frac{\partial \phi}{\partial t} = -\nabla \cdot (\phi \mathbf{v}) + \nabla\left(\frac{\phi(1-\phi)^2}{\zeta}(\nabla \cdot \mathbf{\Pi} - \nabla \cdot \sigma)\right), \qquad (5)$$

$$-\nabla \cdot \mathbf{\Pi} + \nabla \cdot \sigma - \nabla p + \eta \nabla^2 \mathbf{v} = 0. \qquad (6)$$

Here, ζ is the friction constant between polymer and solvent, and η is the viscosity. The pressure p is determined by the incompressible condition: $\nabla \cdot \mathbf{v} = 0$. The stress tensor $\sigma = \sigma_S + \sigma_B \mathbf{I}$ where σ_B is the bulk stress and σ_S is the shear stress tensor. They follow the Maxwell fluid dynamics with the bulk and shear modulus G_B and

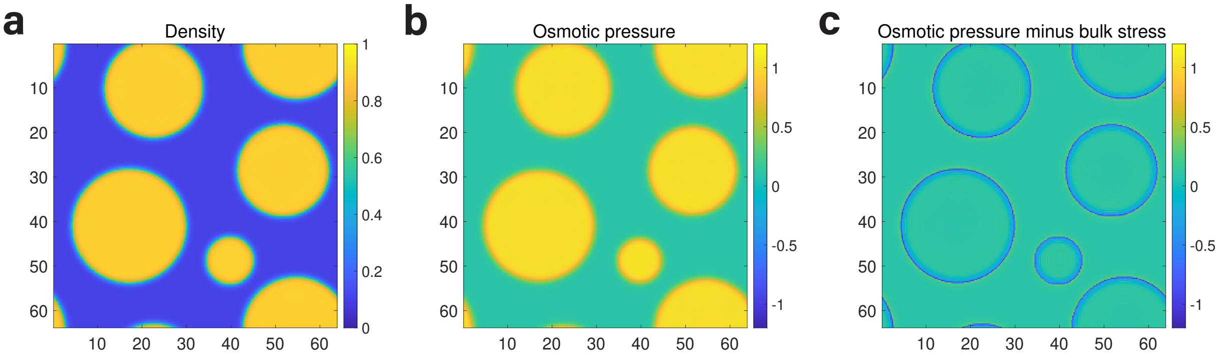

FIG. 2. Simulations of multiple coexisting condensates. (a) The density field ϕ after decreasing χ from 3.0 to 1.5. (b) The osmotic pressure Π from the same simulation of (a). (c) $\Pi - \sigma_B$ from the same simulation of (a). In this figure, we take $\phi_0 = 0.45$, $G_B = 20$, $G_S = 20$, and $\phi_c = 0.5$.

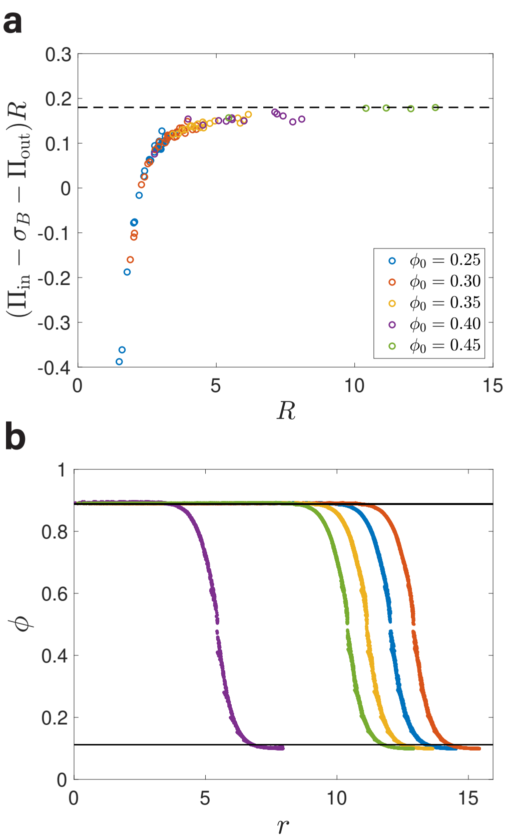

FIG. 3. Computations of the surface tension constant γ and predictions of the density field. (a) The inferred surface tension constant $\gamma = (\Pi_{\text{in}} - \sigma_B - \Pi_{\text{out}})R$ approaches an asymptotic value in the large radius limit. (b) A comparison of the theoretical predictions of ϕ_{in} and ϕ_{out} (black lines) and the simulations in Figure 2(a). Each colored curve represents one condensate and r is the distance from the condensate center. In both (a) and (b), $G_B = 20$, $G_S = 20$, $\phi_c = 0.5$, $\chi_i = 3.0$, $\chi_f = 1.5$. In (b), $\phi_0 = 0.45$.

G_S (Methods). In particular, to simulate elastic condensates, we take the relaxation time of bulk stress to be diverging at a critical density ϕ_c such that

$$\tau_B^{-1}(\phi) = (\phi_c - \phi)\Theta(\phi_c - \phi), \tag{7}$$

where $\Theta(x)$ is the Heaviside function. We remark that if we take the stress tensor to be zero in Eqs. (5, 6), they are reduced to the classical Model H [26]. The osmotic stress tensor is determined by the polymer free energy $f(\phi)$, $\nabla\cdot\mathbf{\Pi} = \phi\nabla f'(\phi)$ where $f(\phi) = f_0(\phi) + \frac{C}{2}(\nabla\phi)^2$ and C is a constant. If not mentioned explicitly, we use the Flory-Huggins free energy: $f_0 = \phi\ln(\phi) + (1-\phi)\ln(1-\phi) + \chi\phi(1-\phi)$. The condition of stable liquid condensate is that the control parameter $\chi > 2$. In this work, we use the osmotic pressure Π to represent the scalar osmotic stress computed from f_0, $\Pi = \phi f_0' - f_0$.

We simulate multiple coexisting elastic condensates by changing χ from $\chi_i = 3$ to $\chi_f = 1.5$. According to our theories, they can be simultaneously stable if each has its osmotic pressure difference balanced by the bulk stress. The density field is indeed uniform inside condensates as assumed (Figure 2a). We also confirm our assumptions of uniform bulk stress and constant radii (Figure S1). Example of simulations are shown in Movie S1. We find that the osmotic pressure is significantly different across the boundaries of condensates (Figure 2b). For liquid condensates, they will quickly dissolve due to the large pressure difference. In contrast, the bulk stress balances the osmotic pressure difference for elastic condensates. Indeed, we find that the $\Pi - \sigma_B$ field is uniform across the boundaries (Figure 2c).

We note that the uniform $\Pi - \sigma_B$ is not valid near the condensate boundaries due to the surface tension. Using the variable sizes of condensates, we compute the radius dependence of surface tension constant γ. We find that γ converges to a constant value in the large radius limit (Figure 3a), suggesting that it is well defined in the thermodynamic limit. We find that the surface tension constant is relatively small in our simulations; therefore, our predictions of the density ϕ_{in} and ϕ_{out} assuming $\gamma =$

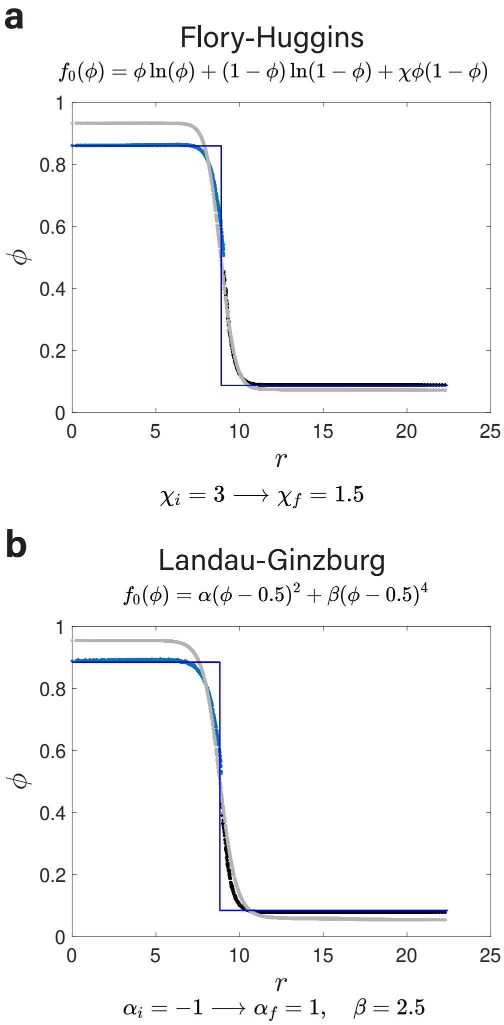

FIG. 4. Simulations using different types of free energy. (a) For the Flory-Huggins free energy, when the control parameter χ decreases from 3.0 to 1.5, the initial density field (gray dots) cannot be maintained and the final density field is established (blue dots). The blue line is the theoretical prediction based on the equilibrium conditions of elastic condensates. (b) For the Landau-Ginzburg free energy, the control parameter α increases from -1 to 1, and the equilibrium density field can also be predicted by our theories. In both (a) and (b), a single condensate is simulated, and $G_S = 20$, $\phi_c = 0.5$, $R_0 = 9$. $G_B = 10$ in (a) and $G_B = 20$ in (b).

0 (Figure 3b) are very close to the predictions with a finite γ (Figure S2). To test the generality of our theories, we also use the Landau-Ginzburg free energy and find that our theories are equally applicable to both forms of free energy (Figure 4). Finally, we also test the effects of shear modulus and critical density, and find that our results are insensitive to the values of G_S and ϕ_c (Figure S3-S6), further corroborating our theories.

Minimum bulk modulus for stable condensates

In the following, we systematically investigate the indissoluble conditions of elastic condensates. We simulate a condensate with two control parameters χ_f and G_B and monitor its dissolution dynamics after χ is reduced from 3 to χ_f. We label the condensate as dissoluble or indissoluble depending on if the system becomes uniform or not after a long waiting time $t = 10^4$ (Figure 5b, c and Movie S2). As expected, when $G_B = 0$, the condensate is stable only if $\chi > 2$. For $\chi < 2$, the condensate becomes indissoluble if the bulk modulus is larger than a critical value ($G_{B,c}$). The results are summarized in the phase diagram (Figure 5a).

We also succeed in finding the theoretically predicted phase boundary separating the dissoluble and indissoluble phase. We compute the theoretically predicted ϕ_{in} as a function of G_B using Eq. (1) with the conservation of total molecular number, and find that ϕ_{in} decreases as G_B decreases (Figure S7). Therefore, a minimum bulk modulus should exist to ensure $\phi_{\text{in}} > \theta\phi_c$ so that the elasticity of the condensate can be maintained. Here, θ is a constant presumably close to 1. We plug $\phi_{\text{in}} = \theta\phi_c$ into Eq. (1) (with ϕ_{out} determined by the conservation of total molecular number) and note that both χ and G_B appear linearly in Eq. (1). Therefore, the phase boundary separating dissoluble and indissoluble phase must be linear in the χ_f-G_B parameter space. Intriguingly, we find that the theoretically computed phase boundary nicely matches the simulated phase diagram (Figure 5a) with $\theta = 1.1$, slightly larger than 1. Our results are not sensitive to the values of ϕ_c as we get similar results using different ϕ_c (Figure S8).

To understand why $\theta \gtrsim 1$, we remark that for the elastic condensate to be stable, ϕ_{in} must be larger than ϕ_c. This is the consequence of force balance across the condensate boundary. The polymer network is subject to two types of force: the force from the gradient of the osmotic tensor ($\nabla \cdot \mathbf{\Pi}$) and the force from the gradient of the elastic stress ($\nabla \cdot \sigma$). We can further decompose the former force into two parts, one is the from the free energy $f_0(\phi)$, which we call as the osmotic force in the following, and the other is from the $\frac{C}{2}(\nabla\phi)^2$ term in the free energy, which we call as the surface tension force in the following. For a liquid condensate, the osmotic force always balances the surface tension force across the condensate boundary. The crossover regime can be separated into three parts in which both the surface tension force and the osmotic force change their signs (see the schematic in Figure 5d and numerical simulations in Figure S9a). For an elastic condensate, the osmotic force always points outwards from the condensates since the chemical potential is now a monotonically increasing function of ϕ. Therefore, in this case, an inward elastic force must exist to balance the sum of surface tension

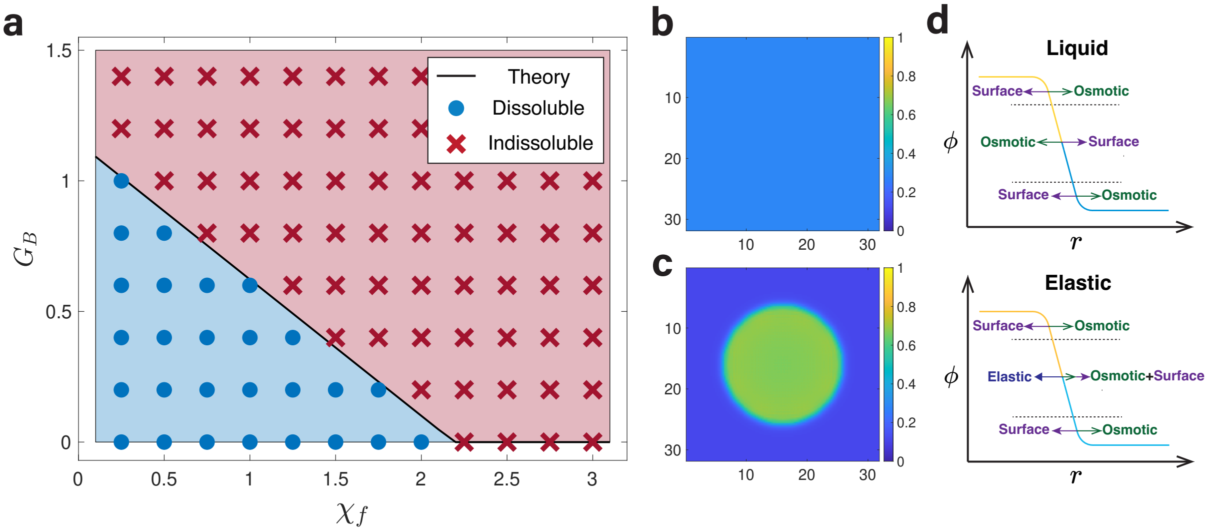

FIG. 5. A critical bulk modulus $G_{B,c}$ above which condensates are indissoluble. (a) Phase diagram of condensate stability with control parameters χ_f and G_B. The theoretical predicted $G_{B,c}$ is the black line and the simulation results are the blue dots and red crosses. (b) and (c) The density fields ϕ for dissolvable and indissoluble cases respectively. In (b), $G_B = 0.4$ and $\chi_f = 0.5$ and the final density is uniform. In (c), $G_B = 1.2$ and $\chi_f = 1.5$ and the condensate is indissoluble due to elasticity. (d) Schematics for the force balance in the crossover regime of condensates.

force and osmotic force in the crossover regime (Figure 5d and Figure S9b). In conclusion, ϕ_{in} should be larger than ϕ_c to ensure a finite elastic force in the crossover regime; therefore, $\theta \gtrsim 1$.

Discussion

While the solid-like nature of biomolecular condensates are largely neglected in theoretical modeling, the elasticity of condensates are crucial to cellular fitness in both positive and negative ways. The conversion of condensates into a solid-like state could help to preserve biological structures and suppress detrimental biochemical reactions [8, 18]. Furthermore, they help to sequester misfolded proteins [22, 30, 31]. On the other hand, the dissolution of solid-like condensates may need assistance by energy-consuming enzymes [16, 32–34], therefore, reducing cellular fitness. Moreover, in conditions where condensates are supposed to dissolve such as the dissolution of stress granules after stress, failure to dissolve may lead to aberrant condensates [8, 18], which further trigger cellular aging and even diseases.

Our work provides the first mechanistic understanding on the irreversible nature of aged biomolecular condensates. We derive the equilibrium conditions of elastic condensates and demonstrate that the bulk stress can balance the osmotic pressure difference inside and outside the condensates, and therefore prevents the dissolution. Our theoretical predictions are nicely confirmed by the numerical simulations using the two-fluid model. Moreover, we both numerically and theoretically obtain a phase diagram of the dissolution conditions of elastic condensates, and obtain a minimum bulk modulus for condensates to be stable upon the condition changes, such as an increase in temperature. There remain some open questions including the effects of shear modulus and finite relaxation times, and we expect future works to explore these questions. Finally, our results may have implications to develop condensate-targeting drugs to specifically change condensate properties inside cells, e.g., lowering the bulk modulus to dissolve irreversible condensates.

METHODS

Derivations of equilibrium conditions

To find the equilibrium condition of elastic condensate, we need to find the change in the elastic energy of a condensate due to a small change in displacement field $\mathbf{u_p} \to \mathbf{u_p} + \delta\mathbf{u_p}$, which can be generally written as

$$\begin{aligned}\delta F_{el} &= \int -\mathbf{f}\cdot\delta\mathbf{u_p}dV = \int -(\nabla\cdot\sigma)\cdot\delta\mathbf{u_p}dV \\ &= \int \sigma\nabla\delta\mathbf{u_p}dV - \int \sigma\delta\mathbf{u_p}d\mathbf{S}.\end{aligned} \tag{8}$$

Here f is the force field and σ is the stress. The above equation shows that the elastic energy change can be generally expressed as the sum of one bulk term and one surface term.

Upon active biological regulation, the attractive interaction between biomolecules become weaker. In the presence of elasticity, the osmotic pressure difference inside and outside the condensate can be balanced by the elastic force, which is generated by the deformation field. We consider a condensate with spherical symmetry and the initial displacement field due to the osmotic pressure difference is radial with constant $\nabla \cdot \mathbf{u_p}$. This generates a dilution of density in bulk of condensate such that $\nabla \cdot \mathbf{u_p} = \log(\phi_1/\phi_{\rm in})$ where ϕ_1 ($\phi_{\rm in}$) is the density before (after) the biological regulation. Note that the stress field inside the condensate is diagonal and also constant $\sigma = \sigma_B \mathbf{I}$.

Now we consider a small change in the volume of the condensate without change in the number of biomolecules. This leads to a change in the density: $\delta\phi/\phi = -\delta V/V$. The resulting change in the displacement field therefore satisfies $\nabla \cdot \delta\mathbf{u_p} = -\delta\phi/\phi = \delta V/V$. Using the spherical symmetry, we obtain $\delta\mathbf{u_p}(r) = r\delta V/(V \cdot d)\mathbf{e_r}$ where d is the spatial dimension and $\mathbf{e_r}$ is the unit radial vector. Therefore, near the surface, the change in the bulk displacement field $\delta\mathbf{u_p}(r \to R) = R\delta V/(V \cdot d)\mathbf{e_r}$. Interestingly, $\delta\mathbf{u_p}(r \to R)$ is just the displacement change needed to increase the volume by δV. This means that the displacement change on the surface is zero, and only the bulk term contributes to the elastic energy change. Therefore, the change in the elastic energy becomes

$$\delta F_{el} = \sigma_B \delta V. \tag{9}$$

Since the free energy changes due to the osmotic pressure and surface tension are the same as the usual liquid condensate, the equilibrium condition due to volume change becomes

$$\Pi_{\rm in} - \sigma_B = \Pi_{\rm out} + \frac{(d-1)\gamma}{R}. \tag{10}$$

Details of the two-fluid model

Numerical simulations of viscoelastic phase separation are based on the two-fluid model [24, 25], which considers the dynamics of polymer velocity $\mathbf{v_p}$, solvent velocity $\mathbf{v_s}$ and the average velocity $\mathbf{v} = \phi\mathbf{v_p} + (1-\phi)\mathbf{v_s}$. This model is derived by minimizing the Rayleighian R of the solution [24, 25, 35], the sum of the energy dissipation function Φ and the temporal changing rate of the free energy $\dot{F}$. The energy dissipation function Φ consists of two parts, which are respectively the friction between polymer and solvent Φ_1, and the overall viscous dissipation of the solution Φ_2

$$\Phi_1 = \int d\mathbf{r}\, \frac{\zeta}{2}(\mathbf{v_p} - \mathbf{v_s})^2 = \int d\mathbf{r}\, \frac{1}{2}\zeta\frac{(\mathbf{v_p} - \mathbf{v})^2}{(1-\phi)^2}, \tag{11}$$

$$\Phi_2 = \int d\mathbf{r}\, \frac{\eta}{4}\big(\nabla\mathbf{v} + (\nabla\mathbf{v})^T\big) : \big(\nabla\mathbf{v} + (\nabla\mathbf{v})^T\big). \tag{12}$$

The temporal changing rate of the mixing free energy $\dot{F}_{\rm mix}$ is calculated through

$$\begin{aligned}\dot{F}_{\rm mix} &= \int d\mathbf{r}\, \dot{\phi} f'(\phi) = \int d\mathbf{r}\, [-\nabla \cdot (\phi\mathbf{v_p})] f'(\phi) \\ &= \int d\mathbf{r}\, [\phi\nabla f'(\phi))] \cdot \mathbf{v_p} = \int d\mathbf{r}\, (\nabla \cdot \mathbf{\Pi}) \cdot \mathbf{v_p},\end{aligned} \tag{13}$$

involving the continuous equation of the density: $\dot{\phi} = -\nabla \cdot (\phi\mathbf{v_p})$. Here $f(\phi) = f_0(\phi) + \frac{C}{2}(\nabla\phi)^2$ and C is a constant. The elastic energy comes from the polymer, so its temporal changing rate is

$$\dot{F}_{\rm el} = \int d\mathbf{r}\, \sigma_{ij}\partial_j v_{p_i} = \int d\mathbf{r}\, (-\nabla \cdot \sigma) \cdot \mathbf{v_p}. \tag{14}$$

Combined with the constrain from the incompressible condition

$$\nabla \cdot \mathbf{v} = 0, \tag{15}$$

and all components mentioned above, the Rayleighian of the solution is therefore:

$$\begin{aligned}R = \int d\mathbf{r}\, \Big[&- p(\nabla \cdot \mathbf{v}) + \frac{\zeta}{2}\frac{(\mathbf{v_p} - \mathbf{v})^2}{(1-\phi)^2} \\ &+ \frac{\eta}{4}\big(\nabla\mathbf{v} + (\nabla\mathbf{v})^T\big) : \big(\nabla\mathbf{v} + (\nabla\mathbf{v})^T\big) \\ &+ (\nabla \cdot \mathbf{\Pi}) \cdot \mathbf{v_p} - (\nabla \cdot \sigma) \cdot \mathbf{v_p}\Big].\end{aligned} \tag{16}$$

By setting the functional derivative of R with $\mathbf{v_p}$ and $\mathbf{v}$ to be 0, we obtain the following equations:

$$\frac{\zeta}{(1-\phi)^2}(\mathbf{v_p} - \mathbf{v}) + \nabla \cdot \mathbf{\Pi} - \nabla \cdot \sigma = 0, \tag{17}$$

$$\nabla p - \frac{\zeta}{(1-\phi)^2}(\mathbf{v_p} - \mathbf{v}) - \eta\nabla^2\mathbf{v} = 0. \tag{18}$$

Finally, we rewrite the above equations and obtain

$$\frac{\partial\phi}{\partial t} = -\nabla \cdot (\phi\mathbf{v_p}), \tag{19}$$

$$\mathbf{v_p} - \mathbf{v} = -\frac{(1-\phi)^2}{\zeta}(\nabla \cdot \mathbf{\Pi} - \nabla \cdot \sigma), \tag{20}$$

$$-\nabla \cdot \mathbf{\Pi} + \nabla \cdot \sigma - \nabla p + \eta\nabla^2\mathbf{v} = 0, \tag{21}$$

Clearly, Eq. (5) is obtained from Eq. (19) and Eq. (20). Combined with the incompressible condition $\nabla \cdot \mathbf{v} = 0$ and Eq. (21), the average velocity $\mathbf{v}$ is calculated as

$$\mathbf{v}(\mathbf{r}) = \int d\mathbf{r}'\, \mathbf{T}(\mathbf{r} - \mathbf{r}') \cdot (-\nabla \cdot \mathbf{\Pi}(\mathbf{r}') + \nabla \cdot \sigma(\mathbf{r}')), \tag{22}$$

while $\mathbf{T}(\mathbf{k}) = \frac{1}{\eta|\mathbf{k}|^2}(\mathbf{I} - \frac{\mathbf{kk}}{|\mathbf{k}|^2})$ is the Oseen tensor in the Fourier space. We can then obtain the polymer velocity $\mathbf{v_p}$ with equation (20). Therefore, the density ϕ in simulation can be updated by calculating $\mathbf{v_p}$ when the osmotic pressure $\mathbf{\Pi}$ and the stress σ are known.

The two components in stress tensor σ, which are shear stress tensor σ_S and bulk stress scalar σ_B, respectively obey the following Maxwell-type equations [25]:

$$\begin{aligned}\frac{\partial \sigma_S}{\partial t} =& -(\mathbf{v_p}\cdot\nabla)\sigma_S + \sigma_S\cdot\nabla\mathbf{v_p} + (\nabla\mathbf{v_p})^T\cdot\sigma_S \\ &- \frac{1}{\tau_S(\phi)}\sigma_S + G_S(\phi)(\nabla\mathbf{v_p} + (\nabla\mathbf{v_p})^T), \quad (23)\\ \frac{\partial \sigma_B}{\partial t} =& -(\mathbf{v_p}\cdot\nabla)\sigma_B - \frac{1}{\tau_B(\phi)}\sigma_B + G_B(\phi)\nabla\cdot\mathbf{v_p}. \quad (24)\end{aligned}$$

In our simulations, we first do not include elastic stress to form condensates by taking $G_S = G_B = 0$. We then introduce the elastic stress by taking

$$G_S(\phi) = G_S\phi^2, \quad (25)$$

$$\tau_S(\phi) = \frac{1}{\phi_c - \phi}\Theta(\phi_c - \phi), \quad (26)$$

$$G_B(\phi) = G_B\Theta(\phi - \phi_c), \quad (27)$$

$$\tau_B(\phi) = \frac{1}{\phi_c - \phi}\Theta(\phi_c - \phi). \quad (28)$$

Here G_B and G_S are constants. We assume a critical density ϕ_c above which the polymer network is percolated and becomes fully elastic with a finite bulk modulus and a diverging relaxation time.

Details of numerical simulations

We perform numerical simulations in a 2D grid by solving the two-fluid model using the explicit Euler method with the periodic boundary condition on MATLAB. Simulations for a single condensate are in a 127×127 grid, and simulations for multiple condensates are in a 255×255 grid. The grid size is $\Delta L = 0.25$ by setting the unit length equal to the lattice size when deriving the mixing free energy. The time interval for the simulation is $\Delta t = 0.001$. In our simulations, we take $k_BT = C = \xi = \eta = 1$ for simplicity. The elastic stress is introduced at $t = 10^3$ for a single condensate and $t = 4\times10^3$ for multiple condensates. The control parameter χ is changed 50 time units after adding the elasticity. Eq. (22) is solved with fast Fourier transformation and other equations are calculated in real space. For the simulation of multiple condensates, we initially add a Gaussian noise with variance 0.001 to the uniform density field. In Figure 5a, simulations are initiated with a single condensate with $R_0 = 9$. The condensate is considered dissoluble if the variance of the ϕ field at $t = 10^4$ is less than 0.01.

[1] C. P. Brangwynne, C. R. Eckmann, D. S. Courson, A. Rybarska, C. Hoege, J. Gharakhani, F. Jülicher, and A. A. Hyman, Germline p granules are liquid droplets that localize by controlled dissolution/condensation, Science **324**, 1729 (2009).

[2] C. P. Brangwynne, P. Tompa, and R. V. Pappu, Polymer physics of intracellular phase transitions, Nature Physics **11**, 899 (2015).

[3] A. Patel, H. O. Lee, L. Jawerth, S. Maharana, M. Jahnel, M. Y. Hein, S. Stoynov, J. Mahamid, S. Saha, T. M. Franzmann, *et al.*, A liquid-to-solid phase transition of the als protein fus accelerated by disease mutation, Cell **162**, 1066 (2015).

[4] Y. Lin, D. S. Protter, M. K. Rosen, and R. Parker, Formation and maturation of phase-separated liquid droplets by rna-binding proteins, Molecular cell **60**, 208 (2015).

[5] S. F. Banani, H. O. Lee, A. A. Hyman, and M. K. Rosen, Biomolecular condensates: organizers of cellular biochemistry, Nature reviews Molecular cell biology **18**, 285 (2017).

[6] J. B. Woodruff, B. F. Gomes, P. O. Widlund, J. Mahamid, A. Honigmann, and A. A. Hyman, The centrosome is a selective condensate that nucleates microtubules by concentrating tubulin, Cell **169**, 1066 (2017).

[7] Y. Shin, J. Berry, N. Pannucci, M. P. Haataja, J. E. Toettcher, and C. P. Brangwynne, Spatiotemporal control of intracellular phase transitions using light-activated optodroplets, Cell **168**, 159 (2017).

[8] T. M. Franzmann, M. Jahnel, A. Pozniakovsky, J. Mahamid, A. S. Holehouse, E. Nüske, D. Richter, W. Baumeister, S. W. Grill, R. V. Pappu, A. A. Hyman, and S. Alberti, Phase separation of a yeast prion protein promotes cellular fitness, Science **359** (2018).

[9] J. Wang, J.-M. Choi, A. S. Holehouse, H. O. Lee, X. Zhang, M. Jahnel, S. Maharana, R. Lemaitre, A. Pozniakovsky, D. Drechsel, *et al.*, A molecular grammar governing the driving forces for phase separation of prion-like rna binding proteins, Cell **174**, 688 (2018).

[10] S. Alberti, A. Gladfelter, and T. Mittag, Considerations and challenges in studying liquid-liquid phase separation and biomolecular condensates, Cell **176**, 419 (2019).

[11] A. S. Lyon, W. B. Peeples, and M. K. Rosen, A framework for understanding the functions of biomolecular condensates across scales, Nature Reviews Molecular Cell Biology **22**, 215 (2021).

[12] L. M. Jawerth, M. Ijavi, M. Ruer, S. Saha, M. Jahnel, A. A. Hyman, F. Jülicher, and E. Fischer-Friedrich, Salt-dependent rheology and surface tension of protein condensates using optical traps, Phys. Rev. Lett. **121**, 258101 (2018).

[13] L. Jawerth, E. Fischer-Friedrich, S. Saha, J. Wang, T. Franzmann, X. Zhang, J. Sachweh, M. Ruer, M. Ijavi, S. Saha, J. Mahamid, A. A. Hyman, and F. Jülicher, Protein condensates as aging maxwell fluids, Science **370**, 1317 (2020).

[14] A. Molliex, J. Temirov, J. Lee, M. Coughlin, A. P. Kanagaraj, H. J. Kim, T. Mittag, and J. P. Taylor, Phase separation by low complexity domains promotes stress granule assembly and drives pathological fibrillization, Cell **163**, 123 (2015).

[15] S. Alberti and A. A. Hyman, Are aberrant phase transitions a driver of cellular aging?, BioEssays **38**, 959 (2016).

[16] J. A. Riback, C. D. Katanski, J. L. Kear-Scott, E. V. Pilipenko, A. E. Rojek, T. R. Sosnick, and D. A. Drummond, Stress-triggered phase separation is an adaptive,

evolutionarily tuned response, Cell **168**, 1028 (2017).

[17] T. S. Harmon, A. S. Holehouse, M. K. Rosen, and R. V. Pappu, Intrinsically disordered linkers determine the interplay between phase separation and gelation in multivalent proteins, eLife **6**, e30294 (2017).

[18] C. Iserman, C. Desroches Altamirano, C. Jegers, U. Friedrich, T. Zarin, A. W. Fritsch, M. Mittasch, A. Domingues, L. Hersemann, M. Jahnel, D. Richter, U.-P. Guenther, M. W. Hentze, A. M. Moses, A. A. Hyman, G. Kramer, M. Kreysing, T. M. Franzmann, and S. Alberti, Condensation of ded1p promotes a translational switch from housekeeping to stress protein production, Cell **181**, 818 (2020).

[19] A. K. Rai, J.-X. Chen, M. Selbach, and L. Pelkmans, Kinase-controlled phase transition of membraneless organelles in mitosis, Nature **559**, 211 (2018).

[20] Y. Shin and C. P. Brangwynne, Liquid phase condensation in cell physiology and disease, Science **357** (2017).

[21] S. Alberti and D. Dormann, Liquid–liquid phase separation in disease, Annual Review of Genetics **53**, 171 (2019), pMID: 31430179.

[22] S. Alberti and A. A. Hyman, Biomolecular condensates at the nexus of cellular stress, protein aggregation disease and ageing, Nature Reviews Molecular Cell Biology **22**, 196 (2021).

[23] J. Berry, C. P. Brangwynne, and M. Haataja, Physical principles of intracellular organization via active and passive phase transitions, Reports on Progress in Physics **81**, 046601 (2018).

[24] H. Tanaka, Viscoelastic phase separation, Journal of Physics: Condensed Matter **12**, R207 (2000).

[25] H. Tanaka and T. Araki, Viscoelastic phase separation in soft matter: Numerical-simulation study on its physical mechanism, Chemical Engineering Science **61**, 2108 (2006).

[26] P. C. Hohenberg and B. I. Halperin, Theory of dynamic critical phenomena, Rev. Mod. Phys. **49**, 435 (1977).

[27] X. Wei, J. Zhou, Y. Wang, and F. Meng, Modeling elastically mediated liquid-liquid phase separation, Phys. Rev. Lett. **125**, 268001 (2020).

[28] Y. Zhang, D. S. W. Lee, Y. Meir, C. P. Brangwynne, and N. S. Wingreen, Mechanical frustration of phase separation in the cell nucleus by chromatin, Phys. Rev. Lett. **126**, 258102 (2021).

[29] P. Ronceray, S. Mao, A. Košmrlj, and M. P. Haataja, Liquid demixing in elastic networks: cavitation, permeation, or size selection? (2021), arXiv:2102.02787 [cond-mat.soft].

[30] D. Kaganovich, R. Kopito, and J. Frydman, Misfolded proteins partition between two distinct quality control compartments, Nature **454**, 1088 (2008).

[31] S. Escusa-Toret, W. I. Vonk, and J. Frydman, Spatial sequestration of misfolded proteins by a dynamic chaperone pathway enhances cellular fitness during stress, Nature cell biology **15**, 1231 (2013).

[32] S. Jain, J. R. Wheeler, R. W. Walters, A. Agrawal, A. Barsic, and R. Parker, Atpase-modulated stress granules contain a diverse proteome and substructure, Cell **164**, 487 (2016).

[33] M. Hondele, R. Sachdev, S. Heinrich, J. Wang, P. Vallotton, B. M. Fontoura, and K. Weis, Dead-box atpases are global regulators of phase-separated organelles, Nature **573**, 144 (2019).

[34] D. Tauber, G. Tauber, A. Khong, B. Van Treeck, J. Pelletier, and R. Parker, Modulation of rna condensation by the dead-box protein eif4a, Cell **180**, 411 (2020).

[35] M. Doi, *Soft matter physics* (Oxford University Press, 2013).